DOI: 10.1002/ejic.200900401

# Ligation of Substituted Pyridines to Metallosalphen Complexes – Crystallographic Characterization of an Unexpected Four-Component Supramolecular Assembly Comprising a Sterically Demanding Ligand

**Eduardo C. Escudero-Adán,[a] Jordi Benet-Buchholz,[a] and Arjan W. Kleij*[a,b]**

**Keywords:** Coordination chemistry / N-heterocyclic ligands / Salen / Supramolecular chemistry / Zinc

The binding properties of various Zn(salphen) complexes with a range of substituted pyridine ligands has been studied in detail using NMR and UV/Vis spectroscopy, X-ray diffraction analysis and molecular modelling studies. The combined results clearly demonstrate that subtle differences in the *ortho*-substitution pattern on the pyridine ring have a dramatic effect on the strength of the Zn–$N_{pyr}$ interaction. In the case of a double *ortho*-substitution, the pyridine donor is unable to bind to the Zn(salphen) complex as a result of the rigid geometry around the Zn ion and the steric repulsion that results upon ligation. The steric requirements of the pyridine ligand infers a preferred positioning of its pendant groups as to minimize repulsive interactions with the salphen ligand. The crystallization of two separate Zn(salphen) complexes in the presence of 2,6-dimethylpyridine has furnished two remarkable 4-component supramolecular structures in which the Zn ion is associated with a water ligand that in turn is surrounded by two pyridine H-bond acceptors; a result that relates to the inability of this pyridine ligand to directly interact with the Zn metal centre.


## Introduction

Salen and similar systems are widely studied as versatile ligands in homogeneous catalysis.[1] Recently, their enormous potential in material applications have also been highlighted.[2] Their efficient use as components of macrocyclic systems,[3] sensors,[4] hybrid materials[5] and multinuclear (cooperative) catalysts[6] has been demonstrated. In this respect, the $Zn^{II}$ centred salens are an important class of synthons since the Lewis acidity of the metal ion can be used in various supramolecular applications by virtue of their strong association with N- and O-donor ligands.[7] We have been active in this area and have been particularly focusing on the use of salphen derivatives [salphen = *N*,*N*′-bis(salicylideneimine)-1,2-phenylenediamine] as synthetically accessible and adaptable molecular (supramolecular) building blocks (Scheme 1).[8] The salphen ligand enforces a rather rigid geometry around the metal ion and in the case of $Zn^{II}$ this leads to a reactive four-coordinate square-planar geometry.[9] As a result, strong axial coordination takes place both in the solid state as well as in solution to allow the formation of more stable square pyrimidal complexes.[10] Previously, we and others[4,11] have demonstrated that the association strength of the fifth apical ligand depends on the steric requirements of the ligand. In this paper we present our findings with regard to the binding of a range of (substituted) N-heterocyclic ligands to Zn(salphen) complexes, and the influence of *ortho* steric bulk present in these latter compounds. The relation between the rigid geometry of the salphen complex and the substitution pattern on the N-heterocycle has been studied using NMR, UV/Vis and X-ray diffraction (XRD) techniques. Together with molecular modeling studies and titration experiments, the scope and limitations of the binding of comparable donor systems will be discussed, and consequently their utility in the formation of functional supramolecular assemblies.

## Results and Discussion

The interaction of N-heterocyclic ligands[12] with various Zn(salphen) complexes was investigated using the pyridine family as a representative case. To obtain an exact 1:1 stoichiometry between the pyridine donors **8**–**14** (Scheme 1) and the Zn(salen) derivatives **1**–**7**, all complexes were crystallized in the presence of the pyridine ligands and the stoichiometry confirmed by $^1$H NMR spectroscopy and elemental analyses (see Exp. Sect.). The 1:1 association was initially assessed by $^1$H NMR in [$D_6$]acetone. Pyridine ligation to the $Zn^{II}$ centre is easily recognized since the close proximity of the pyridine ligand to the salphen backbone produces typical upfield shifts for the *ortho* substituents

[a] Institute of Chemical Research of Catalonia (ICIQ), Av. Països Catalans 16, 43007 Tarragona, Spain
Fax: +34-977-920224
E-mail: akleij@iciq.es
[b] Institució Catalana de Recerca i Estudis Avançats (ICREA), Pg. Lluís Companys 23, 08010 Barcelona, Spain
Supporting information for this article is available on the WWW under http://dx.doi.org/10.1002/ejic.200900401.

  

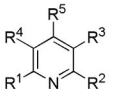

**1**: $R^1 = R^2 = R^3 = R^4 = t$Bu; bridge = phenyl
**2a**: $R^2 = R^3 = t$Bu; $R^1 = R^4$ = H; bridge = phenyl
**2b**: $R^1 = R^4 = t$Bu; $R^2 = R^3$ = H; bridge = phenyl
**3**: $R^1 = R^2 = t$Bu; $R^3 = R^4 = NO_2$; bridge = phenyl
**4**: $R^1 = R^4$ = H; $R^2 = R^3 = t$Bu; bridge = naphthyl
**5**: $R^1 = R^2 = R^3 = t$Bu; bridge = phenyl
**6**: $R^1 = R^4$ = H; $R^2 = R^3$ = OEt; bridge = *c*Hex
**7**: $R^1 = R^2 = R^3 = R^4$ = H; bridge = phenyl

**8**: $R^1 = R^2 = R^3 = R^4 = R^5$ = H
**9**: $R^1 = R^3$ = Me; $R^2 = R^4 = R^5$ = H
**10**: $R^1 = R^2$ = Me; $R^3 = R^4 = R^5$ = H
**11**: $R^1 = R^2 = R^5$ = H; $R^3 = R^4$ = Me
**12**: $R^1 = R^3 = R^4 = R^5$ = H; $R^2$ = Me
**13**: $R^1 = R^3 = R^4 = R^5$ = H; $R^2$ = Et
**14**: $R^1 = R^2 = R^3 = R^4$ = H; $R^5 = t$Bu

Scheme 1. Line drawings of complexes **1**–**7** and pyridine ligands **8**–**14**.

present in the axially ligating molecule (Figure 1).[13] The results of these NMR experiments have been gathered in Table 1.

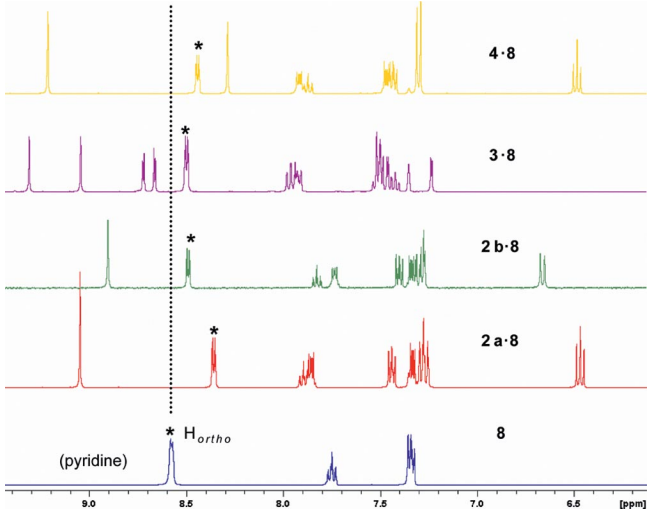


Figure 1. NMR comparison ([$D_6$]acetone) between non-ligated pyridine **8** (bottom) and various 1:1 Zn(salphen)/pyridine complexes at 10–20 mM. The asterisks denote the position of the pyridine-$H_{ortho}$.

The ligation of unsubstituted pyridine **8** provides a reference point for the other 1:1 assemblies. For complexes **1**–**5** the axial coordination of pyridine provokes a typical upfield shift of the *ortho* protons of 0.20–0.25 ppm which is the net result of the electron-withdrawing effect of the Lewis acidic metal centre and the close proximity of the pyridine-$H_{ortho}$ with respect to the salphen aromatic groups (i.e., shielding effect). The substitution of the pyridine ring has a pronounced impact on the positioning of the pyridine ligand in the axial region of the $Zn^{II}$salphen complex.[14] This is illustrated by the NMR spectroscopic data for the assemblies containing pyridine ligands **9**–**14** (Table 1).

Coordination of 2,5-dimethylpyridine (**9**) to Zn(salphen) complex **1** produces a downfield shift for the pyridine-$H_{ortho}$ while the *ortho*-Me fragment is shifted upfield by 0.30 ppm. This indicates that the 2-positioned Me-group is preferentially located in the shielding region of the salphen ligand

Table 1. NMR displacements (in ppm) for the *ortho*-substituents of ligands **8**–**14** upon ligation to Zn(salphen) complexes **1**–**7**: formation of 1:1 assemblies[a] (n.a. = not applicable).

| Complex | Ligand | Assembly | Δδ Pyr-$H_{ortho}$[b] | Δδ Pyr-$CH_3$[b] |
|---|---|---|---|---|
| **1** | **8** | **1·8** | –0.22[c] | n.a. |
| **1** | **9** | **1·9** | +0.15[c] | –0.30[c],[d] |
| **1** | **10** | **1**·$H_2O$·(**10**)$_2$ | n.a. | –0.01[e] |
| **1** | **11** | **1·11** | –0.15 | –0.13 |
| **1** | **12** | **1·12** | –0.03[c] | –0.10[c] |
| **1** | **13** | **1·13** | +0.03 | –0.37[f] |
| **1** | **14** | **1·14** | –0.16 | –0.08[g] |
| **2a** | **8** | **2a·8** | –0.25 | n.a. |
| **2a** | **13** | **2a·13** | –0.01 | –0.21[f] |
| **2a** | **14** | **2a·14** | –0.24 | –0.09 |
| **2b** | **8** | **2b·8** | –0.11 | n.a. |
| **3** | **8** | **3·8** | –0.10 | n.a. |
| **4** | **8** | **4·8** | –0.22 | n.a. |
| **4** | **12** | **4·12** | –0.02 | –0.08 |
| **5** | **8** | **5·8** | –0.21 | n.a. |
| **6** | **8** | **6·8** | [h] | n.a. |
| **7** | **8** | **7·8** | [h] | n.a. |

[a] Measured in [$D_6$]acetone at ambient temperature. [b] The (–) sign indicates an upfield shift as compared to the noncomplexed ligand. [c] See reference 14. [d] Displacement of the *ortho*-$CH_3$. [e] Crystalline material of this complex, with 2 equiv. of the pyridine present per Zn complex (vide infra). [f] Pyridine-$CH_2CH_3$. [g] *tert*-Butylpyridine group. [h] Pyridine complex only soluble in [$D_6$]-DMSO.

(i.e., close to the phenyl rings) and pointing away from the large *t*Bu groups. For the sterically even more demanding 2,6-dimethylpyridine ligand **10** no observable shift is noted for the *ortho*-Me fragments, and in solution weak to no association with complex **1** seems evident (see Supporting Information). For both mono-*ortho*-substituted pyridines 2-methylpyridine **12** and 2-ethylpyridine **13** there also seems to exist a preference for placing the *ortho*-substituent away from the 3- and 3′-*t*Bu groups upon complexation to the Zn complex as illustrated by their upfield shifts. For **12** this effect is somewhat less pronounced. The NMR spectroscopic data of assemblies **2a·13** and **4·12** are in line with those reported for **1·9**.

We also analyzed the 1:1 assemblies based on Zn(salphen) complexes that lack large *t*Bu groups at both 3-positions of the ligand backbone (cf. **2b**, **3** and **7**) to assess whether this directs the assembly formation. For **2b·8** and **3·8** the upfield shifts for the pyridine-$H_{ortho}$ are indeed significantly smaller (–0.11 and –0.10 ppm, respectively, Figure 1) as compared to assemblies **1·8**, **2a·8** and **4·8** (–0.21 to –0.25 ppm) but some care should be taken with the interpretation of these differences. Both complexes **2b** and **3** will have a tendency to form self-assembled dimeric species in solution through $\mu_2$-bridging of one of the salphen-O donor atoms. This phenomenon is well-established for Zn-centred salen complexes with insufficiently large 3- and 3′-positioned groups.[7b] Therefore, the pyridine ligation in these latter examples needs to compete with the Zn(salphen) dimer formation which may cause a smaller observed upfield shift (cf., Figure 1) for the *ortho* groups of the pyridine ligand (**8**). NMR dilution experiments carried out for **3·8** (0.6–33.6 mM range, see Supporting Infor-

  

mation) suggests that the self-association of **3** is relatively strong and hence competes with pyridine complexation. The pyridine complexes based on Zn complexes **6** and **7** proved to be sparingly soluble in most solvents (except for strongly coordinating media such as DMSO) and the data could unfortunately not be used for direct comparison.

The binding of various pyridines to complex **1** and the steric impact upon coordination was further investigated using UV/Vis titrations. The binding curves were fitted using a 1:1 binding model (Table 2).[15] As a reference point the binding of pyridine **8** to Zn(salphen) complex **1** was taken ($K_a = 5.3 \times 10^5$ M$^{-1}$).[14] The addition of double *ortho*-substituted 2,6-dimethylpyridine **10** to Zn(salphen) **1** did not produce any UV/Vis changes reminiscent to a binding event; this corroborates the NMR features of assembly **1**·$H_2O$·(**10**)$_2$ for which no shifts (within experimental error) were noted for the pyridine ligand. Apparently, the presence of *two* rather small *ortho*-Me groups on the pyridine ring is sufficient to completely suppress association to **1**. When the pyridine ligand has only one *ortho*-substituent (i.e., for **9** and **13**) significantly lower association constants are noted for assemblies **1·9** ($K_a = 1.9 \times 10^5$ M$^{-1}$) and **1·13** ($K_a = 0.35 \times 10^5$ M$^{-1}$) as compared to **1·8** regardless the fact that alkylpyridines **9** and **13** should have better donating properties (cf., binding of 3,5-dimethylpyridine to **1**, Table 2). Hence, the UV/Vis titrations follow the same trend as the NMR features, i.e. the more sterically demanding pyridine ligands provoke smaller spectroscopic changes and consequently weaker binding features.

Table 2. UV/Vis titration data of the coordination complexes and association constants using a 1:1 binding model.[a] The association constants are ranked in order of increasing strength.

| Assembly | Pyridine substitution | [complex][b] | $K_a$[c] |
|---|---|---|---|
| **1·10** | 2,6-di-Me | 8.61 | <1[d] |
| **1·13** | 2-Et | 8.94 | 0.35 |
| **1·9** | 2,5-di-Me | 9.10 | 1.9 |
| **1·8**[e] | H | 6.62 | 5.3 |
| **1·11** | 3,5-di-Me | 8.94 | 19.0 |

[a] Measured in pre-dried toluene (anhydrous $Na_2SO_4$) using freshly prepared stock solutions. [b] Concentration: $\times 10^{-5}$ M. [c] $K_a$ = determined association constant ($\times 10^5$ M$^{-1}$ except for **1·10**). [d] No observable changes noted in the UV/Vis spectrum upon addition of the pyridine. [e] See reference [14].

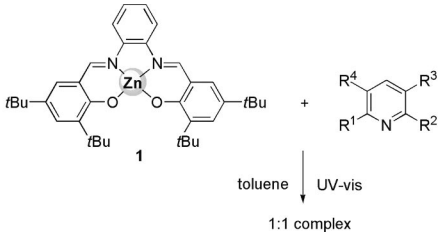


To investigate the pyridine–Zn(salphen) interaction in the solid state, we subjected single crystals obtained from combinations of **1/9**, **1/10** and **3/10** to X-ray diffraction (XRD) analysis. Relevant bond lengths/angles are summarized in Table 3, crystallographic details are summarized in the Exp. Section. All these crystallizations were carried out in warm to hot $CH_3CN$, and suitable crystalline material was obtained by allowing the mixture to cool to ambient temperature. As may be expected, for the combination of complex **1** with 2,5-dimethylpyridine **9** the presence of a 1:1 stoichiometry is observed in the crystal (Figure 2). Interestingly, the 2-positioned methyl group of **9** is located near the bridging phenyl unit, and thus points away from the sterically demanding 3- and 3′-*t*Bu groups of the salphen ligand. This is fully in line with the NMR spectroscopic data that also suggested a preferred positioning of **9** in solution.

Table 3. Selected bond lengths [Å] and angles[°] of assemblies **1·9**, **1**·($H_2O$)·(**10**)$_2$ and **3**·($H_2O$)·(**10**)$_2$; esd values are reported in parentheses.[a]

| | **1·9** | **1**·($H_2O$)·(**10**)$_2$ | **3**·($H_2O$)·(**10**)$_2$ |
|---|---|---|---|
| Zn(1)–O(1) | 1.9855(6) | 1.9632(8) | 2.0022(11) |
| Zn(1)–O(2) | 1.9593(8) | 1.979(8) | 1.9566(10) |
| Zn(1)–O(3) | – | 2.0125(10) | – |
| Zn(1)–O(1 W) | – | – | 2.0110(14) |
| Zn(1)–N(1) | 2.0895(9) | 2.1218(11) | 2.1275(11) |
| Zn(1)–N(2) | 2.0786(7) | 2.091(9) | 2.0540(11) |
| Zn(1)–N(3) | 2.1418(7) | – | – |
| | | | |
| O(2)–Zn(1)–O(1) | 92.36(3) | 95.81(3) | 92.64(4) |
| N(2)–Zn(1)–N(1) | 78.45(3) | 77.30(4) | 78.05(4) |
| O(1)–Zn(1)–N(1) | 88.28(3) | 87.83(4) | 86.88(4) |
| O(1)–Zn(1)–N(2) | 146.50(3) | 155.61(4) | 148.19(5) |
| O(1)–Zn(1)–N(3) | 100.47(3) | – | – |
| O(2)–Zn(1)–N(1) | 160.23(3) | 151.86(4) | 157.07(6) |
| O(2)–Zn(1)–N(2) | 90.41(3) | 88.84(3) | 90.83(4) |
| O(2)–Zn(1)–N(3) | 98.13(3) | – | – |
| N(1)–Zn(1)–N(3) | 101.18(3) | – | – |
| N(2)–Zn(1)–N(3) | 112.16(3) | – | – |
| O(1)–Zn(1)–O* | – | 101.64(4) | 105.21(7) |
| O(2)–Zn(1)–O* | – | 103.74(4) | 105.13(7) |
| O*–Zn(1)–N(1) | – | 102.80(4) | 97.08(6) |
| O*–Zn(1)–N(2) | – | 100.45(4) | 104.34(6) |

[a] The angles that involve the O-atoms of the $H_2O$ ligand are here denoted with an asterisk. For **1**·($H_2O$)·(**10**)$_2$ it concerns O(3) and for **3**·($H_2O$)·(**10**)$_2$ it relates with O(1W).

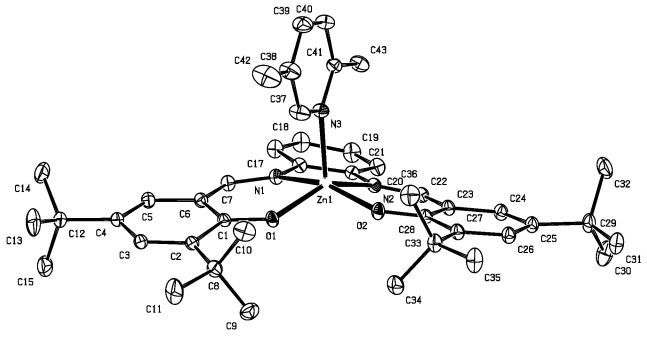


Figure 2. X-ray molecular structure determined for **1·9**. Hydrogen atoms and co-crystallized solvent molecules are omitted for clarity.

The crystallization of **1** in the presence of 2,6-dimethylpyridine (**10**) afforded an unexpected result (Figure 3). In the crystal, the Zn-centre is axially coordinated by a water ligand which in turn is associated (via H-bonding) with two molecules of **10** to form a 4-component supramolecular assembly. The water ligand probably originates from the crystallization solvent ($CH_3CN$). In order to assess whether

  

this result is limited to the use of **1** as complex, we also carried out a similar crystallization of complex **3** in the presence of **10**. As in the case of **1**, a similar 4-component supramolecular assembly was revealed by XRD (Figure 4) showing a potentially wider scope of this interaction pattern between **10** and Zn(salphen) complexes. Between the structures (Table 3) there exist small differences in the coordination geometry around the Zn ion that are imparted by the difference in the positioning of the metal centre above the $N_2O_2$ coordination plane. This is, for instance, illustrated by the Zn(1)–O(1) and Zn(1)–N(2) bond lengths and the angles O(1)–Zn(1)–N(2) and O(2)–Zn(1)–N(1). Such small differences are likely a result of the type of heteroatom that axially coordinates (N- vs. O-ligation) and the interaction of the O-donors with the H-bond acceptors of type **10**.

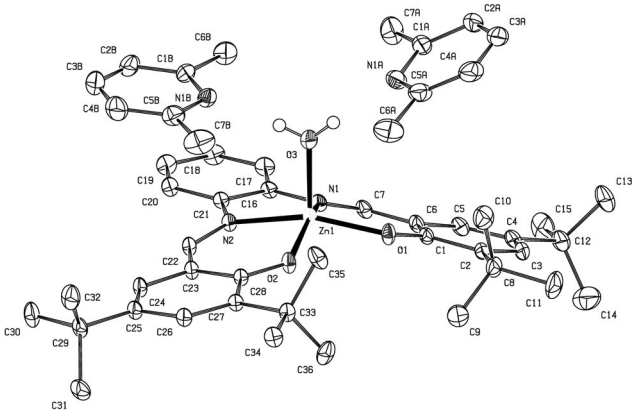


Figure 3. X-ray molecular structure determined for $\mathbf{1}\cdot H_2O\cdot(\mathbf{10})_2$. Hydrogen atoms (except for those of the $H_2O$ ligand) and co-crystallized solvent molecules are omitted for clarity. The pyridines are making hydrogen bonds to the water molecule. Distances: O(3)···N(1A): 2.759(2) Å [uncorrected: N(1A)···H(2W): 1.97 Å] and O(3)···N(1B): 2.704(2) Å [uncorrected: N(1B)···H(1W): 1.89 Å].

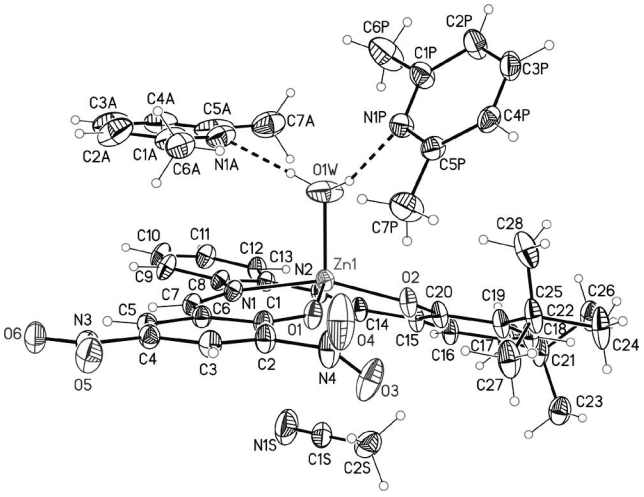


Figure 4. X-ray molecular structure determined for $\mathbf{3}\cdot H_2O\cdot(\mathbf{10})_2$. The positional disorder of one of the pyridine ligands is omitted for clarity.

Further insight into the ability of substituted pyridines to bind to various Zn(salen) complexes was provided by molecular modelling studies (CAChe 7.5 WS, MM2 level, see Supporting Information). First the binding of 2-methylpyridine **12** to Zn(salphen) **1** was examined. The optimized structure shows that the pyridine-methyl group points away from the sterically demanding salphen-*t*Bu groups in line with the $^1$H NMR spectroscopic data for **1·12** and the X-ray analysis performed for **1·9** (cf., position of the 2-methyl group). The introduction of a second pyridine-methyl group at position 6 (i.e., **10**) furnished a calculated structure with a highly distorted tetradentate $N_2O_2$ coordination plane around the Zn metal ion. The latter feature is obviously dictated by the rigid nature of the phenyl bridge group and the salphen ligand is only able to cope with such a coordination pattern by adaptation of an energetically disfavoured geometry. This further rationalizes the NMR, UV/Vis and XRD data obtained for the combinations of **1** with **10**.

When the related Zn(salen) structure (with a bridging *c*-hexyl group) was combined *in silico* with 2-methylpyridine **12** the optimized structure showed the same locational preference for the pyridine-methyl group (see Supporting Information). Thus it seems that the bulky *t*Bu groups of the sal(ph)en ligands have a predominant influence on the geometry of the Zn(salen)–pyridine assemblies. This is further supported by the energy-minimized structures for assemblies based on Zn(salphen) **2b** (Scheme 1) that lacks the 3- and 3′-*t*Bu groups. In the calculated structure **2b·12** the pyridine-methyl fragment points in the opposite direction as compared to the calculated structure **1·12**, i.e. away from the bridging phenyl group (Supporting Information). For the assembly **2b·10**, based on the binding of 2,6-dimethylpyridine, the distortion of the $N_2O_2$ coordination plane upon ligation of **10** to **2b** is much less as referred to assembly **1·10**.

Other bridging groups such as alkyl chains ($\geq C_2$) give rise to Zn(salen) structures that have increasing trigonal bipyramidal character and are more flexible to accommodate the ligation of sterically demanding pyridines such as **10**. In these cases there seems less preference for a preferred positioning of the methyl substituents close to the bridging group in the 1:1 assemblies.

## Conclusions

In this work we have detailed the relationship between the rigid coordination geometry of salphen type ligands around $Zn^{II}$ ions and its influence on the axial coordination ability of various, substituted pyridines as a representative family of N-heterocycles. Subtle differences in the *ortho* groups present next to the heteroatom lead to significantly different coordination complexes. In the case of 2,6-dimethylpyridine, a remarkable four-component supramolecular assembly was crystallographically characterized. In this system, the N-heterocycle is unable to coordinate directly to the $Zn^{II}$ ion due to strong steric infringement of the salphen geometry around the metal centre upon formation of the

  

1:1 complex. Instead, during the crystallization process a water molecule is axially bound which in turn forms hydrogen bridges to two pyridine units. The strength of the Zn–$N_{pyr}$ in salphen derivatives is therefore a function of the substitution pattern on the N-heterocycle and particularly sensitive to (double) *ortho* substitution, which is supported by molecular modelling studies, NMR and UV/Vis titration data, and XRD studies. However, the strength of the supramolecular coordination motif is also dependent on the ability of the salen bridging group to facilitate geometrical changes upon enforcing the Zn–$N_{pyr}$ interaction (cf., molecular modelling studies). Clearly, for salphen complexes there is little degree of freedom to accommodate ligation of pyridine ligands with bulky (*ortho*) substituents. Therefore, a successful use and fine-tuning of the Zn(salen)–N coordination pattern in the build up of more complicated noncovalent architectures will depend on a delicate balance between the steric requirements of the guest molecule (e.g., N-heterocycles) and the flexibility of the host system (Zn-salen). We are currently focusing on such systems with the implementation of the principles here communicated.

## Experimental Section

**General:** The Zn complexes **1**,[9] **2a**,[9] **2b**,[16] **3**,[16] **4**,[8a] **6**[17] and **7**[18] and mono-imine **A**[19] (see Supporting Information for structures) were prepared according to procedures that were previously reported. All pyridine compounds were purchased and used without further purification. NMR measurements were carried out on a Varian 400 MHz spectrometer using TMS as an internal standard. UV/Vis measurements were recorded on a Shimadzu UV-1700 PharmaSpec spectrofotometer. MS studies were performed by the Research Support unit from the ICIQ. Elemental analyses were carried at the Unidad de Análisis Elemental of the University of Santiago de Compostela (Spain).

**5:** To a solution of monoimine **A** (0.47 g, 1.45 mmol) in MeOH (30 mL) was first added 3-*tert*-butylsalicylaldehyde (0.31 g, 1.74 mmol) and then a solution of $Zn(OAc)_2{\cdot}2H_2O$ (1.22 g, 5.56 mmol) dissolved in MeOH (10 mL). The resultant yellow solution was stirred for 3 d and then filtered to furnish a yellow solid. The filtrate was cooled stepwise to 6 °C and –25 °C to yield more fractions of the title compound. Total yield 476.6 mg (0.870 mmol, 60% based on **A**). $^1$H NMR (400 MHz, [D$_6$]acetone): $\delta$ = 9.11 (s, 1 H, CH=N), 9.06 (s, 1 H, CH=N), 7.89–7.94 (m, 2 H, ArH), 7.44 (d, $^4J$ = 2.7 Hz, 1 H, ArH), 7.34–7.39 (m, 2 H, ArH), 7.26–7.31 (m, 3 H, ArH), 6.49 (t, $^3J$ = 7.6 Hz, 1 H, ArH), 1.55 [s, 9 H, C(CH$_3$)$_3$], 1.53 [s, 9 H, C(CH$_3$)$_3$], 1.33 [s, 9 H, C(CH$_3$)$_3$] ppm. $^{13}$C{$^1$H} NMR [10 MHz, (D$_6$)acetone + 5% (D$_5$)pyridine]: $\delta$ = 173.90, 172.32, 164.21, 163.80, 143.05, 142.44, 141.31, 140.95, 135.38, 134.74, 131.57, 130.53, 130.07, 127.89, 127.64, 120.64, 119.41, 116.84, 116.81, 113.38, 36.35, 36.07, 34.49, 31.87, 30.29, 30.17 ppm. MS (MALDI+, pyrene): *m*/*z* = 546.3 (M)$^+$. $C_{32}H_{38}N_2O_2Zn{\cdot}0.5H_2O$ (557.08): calcd. C 68.99, H 7.06, N 5.03; found C 68.68, H 6.71, N 5.10.

**1·8:** A mixture of complex **1** (57.8 mg, 0.0957 mmol) and pyridine ligand **8** (0.5 mL) was combined in hot acetonitrile (5 mL). The orange solution was cooled upon which yellow to orange crystalline material deposited in due course. The crystals were collected by filtration, washed with hexane and dried. Yield 47.5 mg (0.0695 mmol, 73%). $^1$H NMR (400 MHz, [D$_6$]acetone): $\delta$ = 9.07 (s, 2 H, CH=N), 8.38 (m, 2 H, Pyr-H$_{ortho}$), 7.86–7.89 (m, 3 H, ArH + Pyr-H$_{para}$), 7.42–7.46 (m, 4 H, ArH + Pyr-H$_{meta}$), 7.30–7.33 (m, 2 H, ArH), 7.24 (d, $^4J$ = 2.7 Hz, 2 H, ArH), 1.53 [s, 18 H, C(CH$_3$)$_3$], 1.32 [s, 18 H, C(CH$_3$)$_3$] ppm. $C_{41}H_{51}N_3O_2Zn$ (683.27): calcd. C 72.07, H 7.52, N 6.15; found C 72.25, H 7.97, N 6.16.

**1·H$_2$O·(10)$_2$:** Compound **1** (71.1 mg, 0.118 mmol) and **10** (0.5 mL) in $CH_3CN$ (8 mL) were shortly heated to reflux. In due course, orange needles deposited which were collected by decantation and dried. Another two crops of crystalline material were obtained at –28 °C, total yield 59.7 mg (0.0714 mmol, 60%). These crystals were suitable for XRD analysis. $^1$H NMR (400 MHz, [D$_6$]acetone): $\delta$ = 9.09 (s, 2 H, CH=N), 7.89–7.92 (m, 2 H, ArH), 7.49 (t, $^3J$ = 7.7 Hz, 2 H, Pyr-H$_{para}$), 7.44 (d, $^4J$ = 2.7 Hz, 2 H, ArH), 7.33–7.35 (m, 2 H, ArH), 7.24 (d, $^4J$ = 2.7 Hz, 2 H, ArH), 6.99 (d, $^3J$ = 7.6 Hz, 4 H, Pyr-H$_{meta}$), 2.42 (s, 12 H, Pyr-CH$_3$), 1.54 [s, 18 H, C(CH$_3$)$_3$], 1.32 [s, 18 H, C(CH$_3$)$_3$] ppm. $C_{50}H_{66}N_4O_3Zn$ (836.49): calcd. C 71.79, H 7.95, N 6.70; found C 72.07, H 7.89, N 6.66.

**1·11:** The procedure reported for **1·8** was followed using **1** (52.9 mg, 0.0876 mmol) and **11** (0.5 mL) in $CH_3CN$ (5 mL). Orange to red crystals, yield 42.1 mg (0.0592 mmol, 68%). $^1$H NMR (400 MHz, [D$_6$]acetone): $\delta$ = 9.04 (s, 2 H, CH=N), 8.06 (m, 2 H, Pyr-H$_{ortho}$), 7.85–7.88 (m, 2 H, ArH), 7.51 (m, 1 H, Pyr-H$_{para}$), 7.43 (d, $^4J$ = 2.7 Hz, 2 H, ArH), 7.32–7.34 (m, 2 H, ArH), 7.22 (d, $^4J$ = 2.7 Hz, 2 H, ArH), 2.14 (s, 6 H, Pyr-CH$_3$), 1.54 [s, 18 H, C(CH$_3$)$_3$], 1.31 [s, 18 H, C(CH$_3$)$_3$] ppm. $C_{43}H_{55}N_3O_2Zn$ (711.33): calcd. C 72.61, H 7.79, N 5.91; found C 72.51, H 8.07, N 6.01.

**1·13:** The procedure reported for **1·8** was followed using **1** (127.7 mg, 0.211 mmol) and **13** (0.5 mL) in $CH_3CN$ (5 mL). The orange crystalline product was obtained at –28 °C. Yield 75.2 mg (0.106 mmol, 50%). $^1$H NMR (400 MHz, [D$_6$]acetone): $\delta$ = 9.03 (s, 2 H, CH=N), 8.50 (d, $^3J$ = 4.4, $^4J$ = 0.8 Hz, 1 H, Pyr-H$_{ortho}$), 7.83–7.85 (m, 2 H, ArH), 7.73 (t, $^3J$ = 7.7, $^4J$ = 1.8 Hz, 1 H, Pyr-H$_{para}$), 7.45 (d, $^4J$ = 2.7 Hz, 2 H, ArH), 7.31–7.33 (m, 2 H, ArH), 7.27 (d, $^3J$ = 7.9 Hz, 1 H, Pyr-H$_{meta}$), 7.24 (d, $^4J$ = 2.7 Hz, 2 H, ArH), 7.18 (t, $^3J$ = 6.4 Hz, 1 H, Pyr-H$_{meta}$), 2.73 (q, $^3J$ = 7.6 Hz, 2 H, Pyr-C$H_2$CH$_3$), 1.52 [s, 18 H, C(CH$_3$)$_3$], 1.32 [s, 18 H, C(CH$_3$)$_3$], 2.73 (t, $^3J$ = 7.6 Hz, 3 H, Pyr-CH$_2$C$H_3$) ppm. $C_{43}H_{55}N_3O_2Zn$ (711.33): calcd. C 72.61, H 7.79, N 5.91; found C 72.78, H 8.07, N 5.88.

**1·14:** The procedure reported for **1·8** was followed using **1** (32.1 mg, 0.0531 mmol) and **14** (0.1 mL) in $CH_3CN$ (2 mL). Orange microcrystalline solid, yield 30.1 mg (0.0407 mmol, 77%). $^1$H NMR (400 MHz, [D$_6$]acetone): $\delta$ = 9.07 (s, 2 H, ArH), 8.25 (d, $^3J$ = 5.0, $^4J$ = 1.6 Hz, 2 H, Pyr-H$_{ortho}$), 7.87–7.89 (m, 2 H, ArH), 7.47 (d, $^3J$ = 5.0, $^4J$ = 1.6 Hz, 2 H, Pyr-H$_{meta}$), 7.42 (d, $^4J$ = 2.7 Hz, 2 H, ArH), 7.31–7.33 (m, 2 H, ArH), 7.22 (d, $^4J$ = 2.7 Hz, 2 H, ArH), 1.53 [s, 18 H, C(CH$_3$)$_3$], 1.31 [s, 18 H, C(CH$_3$)$_3$], 1.23 [s, 9 H, Pyr-C(CH$_3$)$_3$] ppm. $C_{45}H_{59}N_3O_2Zn{\cdot}0.5H_2O$ (748.39): calcd. C 72.22, H 8.08, N 5.61; found C 72.04, H 7.94, N 5.56.

**2a·8:** The procedure reported for **1·8** was followed using **2** (91.1 mg, 0.185 mmol) and **8** (0.5 mL) in $CH_3CN$ (5 mL). Yellow to orange crystalline material, yield 72.2 mg (0.126 mmol, 68%). $^1$H NMR (400 MHz, [D$_6$]acetone): $\delta$ = 9.05 (s, 2 H, CH=N), 8.36 (m, 2 H, Pyr-H$_{ortho}$), 7.84–7.89 (m, 3 H, ArH + Pyr-H$_{para}$), 7.42–7.46 (m, 2 H, Pyr-H$_{meta}$), 7.32–7.34 (m, 2 H, ArH), 7.25–7.30 (m, 4 H, ArH), 6.47 (t, $^3J$ = 7.7 Hz, 2 H, ArH), 1.50 [s, 18 H, C(CH$_3$)$_3$] ppm. $C_{33}H_{35}N_3O_2Zn{\cdot}0.5CH_3CN$ (591.59): calcd. C 69.03, H 6.22, N 8.29; found C 68.82, H 5.92, N 8.18.

**2a·13:** The procedure reported for **1·8** was followed using **2** (155.7 mg, 0.258 mmol) and **13** (288.4 mg, 2.69 mmol) in $CH_3CN$ (10 mL). Orange, block-shaped crystals were isolated, yield 139.2 mg (0.196 mmol, 76%). $^1$H NMR (400 MHz, [D$_6$]acetone): $\delta$

  

= 9.01 (s, 2 H, CH=N), 8.46 (m, 1 H, Pyr-$H_{ortho}$), 7.82–7.85 (m, 2 H, ArH), 7.75 (t, $^3J$ = 7.7, $^4J$ = 1.8 Hz, 1 H, Pyr-$H_{para}$), 7.33–7.35 (m, 2 H, ArH), 7.26–7.31 (m, 5 H, ArH + Pyr-H), 7.17–7.20 (m, 1 H, Pyr-H), 6.48 (t, $^3J$ = 7.6 Hz, 2 H, ArH), 2.73 (q, $^3J$ = 7.6 Hz, 2 H, Pyr-C$H_2$CH$_3$), 1.49 [s, 18 H, C(CH$_3$)$_3$], 1.04 (t, $^3J$ = 7.6 Hz, 3 H, Pyr-CH$_2$C$H_3$) ppm. $C_{35}H_{39}N_3O_2Zn$ (599.11): calcd. C 70.17, H 6.56, N 7.01; found C 70.13, H 6.40, N 7.20.

**2a·14:** The procedure reported for **1·8** was followed using **2** (220.5 mg, 0.448 mmol) and **14** (10 drops) in $CH_3CN$ (5 mL). A yellow to orange micro-crystalline solid was obtained from hexane at –28 °C, yield 195.8 mg (0.312 mmol, 70%). $^1$H NMR (400 MHz, [D$_6$]acetone): $\delta$ = 9.05 (s, 2 H, CH=N), 8.23 (d, $^3J$ = 5.0, $^4J$ = 1.6 Hz, 2 H, Pyr-$H_{ortho}$), 7.86–7.88 (m, 2 H, ArH), 7.47 (d, $^3J$ = 5.0, $^4J$ = 1.6 Hz, 2 H, Pyr-$H_{meta}$), 7.32–7.35 (m, 2 H, ArH), 7.24–7.29 (m, 4 H, ArH), 6.45 (t, $^3J$ = 7.6 Hz, 2 H, ArH), 1.50 [s, 18 H, C(CH$_3$)$_3$], 1.23 [s, 18 H, Pyr-C(CH$_3$)$_3$] ppm. $C_{37}H_{43}N_3O_2Zn$ (627.17): calcd. C 70.86, H 6.91, N 6.70; found C 70.07, H 6.89, N 6.72.

**2b·8:** The procedure reported for **1·8** was followed using **2b** (34.6 mg, 0.0703 mmol) and **8** (1 mL) in $CH_3CN$ (10 mL). Yellow needles were isolated, yield 22.8 mg (0.0399 mmol, 57%). $^1$H NMR (400 MHz, [D$_6$]acetone): $\delta$ = 8.90 (s, 2 H, CH=N), 8.49 (m, 2 H, Pyr-$H_{ortho}$), 7.83 (s, 1 H, Pyr-$H_{para}$), 7.72–7.75 (m, 2 H, ArH), 7.38–7.42 (m, 2 H, ArH), 7.26–7.34 (m, 6 H, ArH + Pyr$H_{meta}$), 6.66 (d, $^3J$ = 8.8 Hz, 2 H, ArH), 1.27 [s, 18 H, C(CH$_3$)$_3$] ppm. $C_{33}H_{35}N_3O_2Zn{\cdot}0.5H_2O$ (580.07): calcd. C 68.33, H 6.26, N 7.24; found C 68.39, H 5.92, N 7.25.

**3·8:** The procedure reported for **1·8** was followed using **3** (44.9 mg, 0.0772 mmol) and **8** (0.5 mL) in $CH_3CN$ (5 mL). The product was isolated by concentration, addition of hexane and decantation. Orange solid, yield 38.7 mg (0.0585 mmol, 76%). $^1$H NMR (400 MHz, [D$_6$]acetone): $\delta$ = 9.31 (s, 1 H, CH=N), 9.05 (s, 1 H, CH=N), 8.72 (d, $^4J$ = 3.1 Hz, 1 H, ArH), 8.66 (d, $^4J$ = 3.1 Hz, 1 H, ArH), 8.49–8.51 (m, 2 H, Pyr-$H_{ortho}$), 7.91–7.98 (m, 3 H, ArH + Pyr-$H_{para}$), 7.40–7.54 (m, 5 H, ArH + Pyr-$H_{meta}$), 7.24 (d, $^4J$ = 2.6 Hz, 1 H, ArH), 1.49 [s, 18 H, C(CH$_3$)$_3$], 1.30 [s, 18 H, C(CH$_3$)$_3$] ppm. $C_{33}H_{35}N_5O_6Zn$ (661.06): calcd. C 59.96, H 5.03, N 10.59; found C 59.65, H 5.18, N 10.63.

**4·8:** The procedure reported for **1·8** was followed using **4** (70.5 mg, 0.130 mmol) and **8** (0.5 mL) in $CH_3CN$ (5 mL). Orange crystals were obtained at –28 °C, yield 51.0 mg (0.0821 mmol, 63%). $^1$H NMR (400 MHz, [D$_6$]acetone): $\delta$ = 9.21 (s, 2 H, CH=N), 8.44 (m, 2 H, Pyr-$H_{ortho}$), 8.29 (s, 2 H, ArH), 7.91–7.93 (m, 2 H, ArH), 7.85–7.89 (m, 1 H, Pyr-$H_{para}$), 7.45–7.48 (m, 2 H, ArH), 7.41–7.44 (m, 2 H, Pyr-$H_{meta}$), 7.30 (d, $^3J$ = 7.6 Hz, 4 H, ArH), 6.48 (t, $^3J$ = 7.6 Hz, 2 H, ArH), 1.50 [s, 18 H, C(CH$_3$)$_3$] ppm. $C_{37}H_{37}N_3O_2Zn$ (621.12): calcd. C 71.55, H 6.00, N 6.77; found C 71.21, H 6.04, N 6.70.

**4·12:** The procedure reported for **1·8** was followed using **4** (48.1 mg, 0.0887 mmol) and **12** (0.5 mL) in $CH_3CN$ (5 mL). Yellow crystals were obtained at –28 °C, yield 37.4 mg (0.0589 mmol, 66%). $^1$H NMR (400 MHz, [D$_6$]acetone): $\delta$ = 9.14 (s, 2 H, CH=N), 8.43 (d, $^3J$ = 5.3, $^4J$ = 0.9 Hz, 1 H, Pyr-$H_{ortho}$), 8.21 (s, 2 H, ArH), 7.88–7.92 (m, 2 H, ArH), 7.72 (t, $^3J$ = 7.7, $^4J$ = 1.8 Hz, 1 H, Pyr-$H_{para}$), 7.44–7.48 (m, 2 H, ArH), 7.32 (d, $^3J$ = 7.3 Hz, 4 H, ArH), 7.25 (d, $^3J$ = 7.8 Hz, 1 H, Pyr-H), 7.20 (pseudo t, $^3J$ = 6.4 Hz, 1 H, Pyr-H), 6.50 (t, $^3J$ = 7.6 Hz, 2 H, ArH), 2.40 (s, 3 H, Pyr-CH$_3$), 1.49 [s, 18 H, C(CH$_3$)$_3$] ppm. $C_{38}H_{39}N_3O_2Zn$ (635.15): calcd. C 71.86, H 6.19, N 6.62; found C 71.51, H 6.06, N 6.59.

**5·8:** The procedure reported for **1·8** was followed using **5** (51.7 mg, 0.0943 mmol) and **8** (0.5 mL) in $CH_3CN$ (5 mL). The compound was isolated by drying in vacuo and washing the residue with a minimum amount of cold hexane. Orange solid, yield 46.5 mg (0.0741 mmol, 79%). $^1$H NMR (400 MHz, [D$_6$]acetone): $\delta$ = 9.10 (s, 1 H, CH=N), 9.05 (s, 1 H, CH=N), 8.38 (m, 2 H, Pyr-$H_{ortho}$), 7.85–7.93 (m, 3 H, ArH + Pyr-$H_{para}$), 7.44–7.48 (m, 3 H, ArH), 7.27–7.37 (m, 5 H, ArH + Pyr-$H_{meta}$), 6.47 (t, $^3J$ = 7.7 Hz, 1 H, ArH), 1.54 [s, 9 H, C(CH$_3$)$_3$], 1.51 [s, 9 H, C(CH$_3$)$_3$], 1.34 [s, 9 H, C(CH$_3$)$_3$] ppm. $C_{37}H_{43}N_3O_2Zn{\cdot}0.5H_2O$ (666.25): calcd. C 69.85, H 6.97, N 6.61; found C 69.59, H 7.13, N 6.42.

**6·8:** The procedure reported for **1·8** was followed using **6** (49.3 mg, 0.104 mmol) and **8** (3 mL) in $CH_3CN$ (5 mL). Light-yellow block-shaped crystals were isolated in two fractions (at room temp. and –28 °C), total yield amounted to 44.6 mg (0.0807 mmol, 78%). $^1$H NMR (400 MHz, [D$_6$]DMSO): $\delta$ = 8.57 (m, 2 H, Pyr-$H_{ortho}$), 8.32 (s, 2 H, CH=N), 7.79 (m, 1 H, Pyr-$H_{para}$), 7.39 (m, 2 H, Pyr-$H_{meta}$), 6.85 (d, $^3J$ = 7.9, $^4J$ = 1.6 Hz, 2 H, ArH), 6.78 (d, $^3J$ = 7.6, $^4J$ = 1.5 Hz, 2 H, ArH), 6.32 (t, $^3J$ = 7.7 Hz, 2 H, ArH), 3.96–4.05 (m, 4 H, Ar-OC$H_2$CH$_3$), 3.17 (m, 2 H, *c*-hexyl-H), 2.43–2.45 (m, 2 H, *c*-hexyl-H), 1.89 (m, 2 H, *c*-hexyl-H), 1.38 (m, 4 H, *c*-hexyl-H), 1.32 (t, $^3J$ = 7.0 Hz, 6 H, Ar-OCH$_2$C$H_3$) ppm. $C_{29}H_{33}N_3O_4Zn{\cdot}H_2O$ (571.02): calcd. C 61.00, H 6.18, N 7.36; found C 61.18, H 6.14, N 6.99.

**7·8:** The procedure reported for **1·8** was followed using **7** (34.7 mg, 0.0914 mmol) and **8** (4 mL) in $CH_3CN$ (8 mL). Yellow crystals were obtained at –28 °C, yield 19.6 mg (0.0427 mmol, 47%). $^1$H NMR (400 MHz, [D$_6$]DMSO): $\delta$ = 9.01 (s, 2 H, CH=N), 8.56 (m, 2 H, Pyr-$H_{ortho}$), 7.87–7.91 (m, 2 H, ArH), 7.83 (m, 1 H, Pyr-$H_{para}$), 7.37–7.43 (m, 6 H, ArH + Pyr-$H_{meta}$), 7.24 (t, $^3J$ = 7.7, $^4J$ = 1.9 Hz, 2 H, ArH), 6.70 (d, $^3J$ = 8.2 Hz, 2 H, ArH), 6.51 (t, $^3J$ = 7.3, $^4J$ = 1.0 Hz, 2 H, ArH) ppm. $C_{25}H_{19}N_3O_2Zn$ (458.85): calcd. C 65.44, H 4.17, N 9.16; found C 65.55, H 4.36, N 9.29.

**Crystal Data for 1·9:** Formula $C_{43}H_{55}N_3O_2Zn$, $M$ = 711.27, triclinic, $P\bar{1}$, $a$ = 10.8412(6) Å, $b$ = 12.5699(6) Å, $c$ = 15.9140(8) Å, $\alpha$ = 82.272(2)°, $\beta$ = 79.102(2)°, $\gamma$ = 64.875(3)°, $V$ = 1924.46(17) Å$^3$, $Z$ = 2, $\rho$(calcd.) = 1.227 g/cm$^3$, $F$(000) = 760, crystal size: 0.30 × 0.30 × 0.10 mm$^3$, $T$ [K] = 100(2), $\theta_{min./max.}$ = 2.71–39.88°, total/unique data: 35622/16131, $R$(int) = 0.021, data/restraints/parameters: 16131/0/456, GOF = 1.038, $R_1$ = 0.0329 and $wR_2$ = 0.0870 [$I > 2\sigma(I)$], min. and max. residual densities: –0.279, 0.884 [e/Å$^3$].

**Crystal Data for 1·H$_2$O·(10)$_2$:** Formula $C_{50}H_{66}N_4O_3Zn$, $M$ = 836.44, monoclinic, $P2_1/c$, $a$ = 11.6858(5) Å, $b$ = 28.2958(12) Å, $c$ = 14.7641(6) Å, $\beta$ = 105.599(2)°, $V$ = 4702.1(3) Å$^3$, $Z$ = 4, $\rho$(calcd.) = 1.182 g/cm$^3$, $F$(000) = 1792, crystal size: 0.30 × 0.30 × 0.10 mm$^3$, $T$ [K] = 100(2), $\theta_{min./max.}$ = 2.82–39.87°, total/uniqe data: 27421/18320, $R$(int) = 0.0739, data/restraints/parameters: 27421/0/547, GOF = 1.031, $R_1$ = 0.0602 and $wR_2$ = 0.1415 [$I > 2\sigma(I)$], min. and max. residual densities: –2.029, 1.676 [e/Å$^3$].

**Crystal Data for 3·H$_2$O·(10)$_2$:** Formula $C_{44}H_{51}N_7O_7Zn$, $M$ = 855.29, monoclinic, $C2/c$, $a$ = 42.1120(12) Å, $b$ = 10.3564(3) Å, $c$ = 24.5257(7) Å, $\beta$ = 122.1990(10)°, $V$ = 9051.3(4) Å$^3$, $Z$ = 8, $\rho$(calcd.) = 1.255 g/cm$^3$, $F$(000) = 3600, crystal size 0.30 × 0.20 × 0.10 mm$^3$, $T$ [K] = 100(2), $\theta_{min./max.}$ = 3.04–39.69°, total/uniqe data: 101374/26881, $R$(int) = 0.0353, data/restraints/parameters: 26881/57/569, GOF = 1.026, $R_1$ = 0.0587 and $wR_2$ = 0.1751 [$I > 2\sigma(I)$], min. and max. residual densities: –0.818, 2.040 [e/Å$^3$]. *Comments*: The unit cell contains one molecule of Zn complex attached to a water molecule, one molecule of $CH_3CN$ and two molecules of the pyridine (2,6-dimethylpyridine) forming hydrogen bonds to the water molecule. One of the pyridine molecules is disordered in four different sites (occupation: 26.5/25.2/28.4/19.8). These disordered pyridine molecules are additionally overlapping with the same disordered

  

molecules attached to the neighbouring Zn atoms leading to a complicated disorder model.

CCDC-725183 (for **1·9**), -725184 [for **1**·$H_2O$·(**10**)$_2$] and -725185 [for **3**·$H_2O$·(**10**)$_2$] contain the supplementary crystallographic data for this paper. These data can be obtained free of charge from The Cambridge Crystallographic Data Centre via www.ccdc.cam.ac.uk/data_request/cif.

**Supporting Information** (see also the footnote on the first page of this article): Molecular modeling results, copies of NMR spectra, UV/Vis titration data and line drawing of compound **A**.

## Acknowledgments

The authors wish to thank the Institució Catalana de Recerca i Estudis Avançats (ICREA) and the Institute of Chemical Research of Catalonia (ICIQ) for generous support to this work (A. W. K. is an ICREA fellow). The Spanish Ministerio de Educación y Ciencias (MEC) is also thanked for a financial contribution through project number CTQ2008-02050/BQU. Dr. Noemí Cabello is thanked for the mass spectrometric studies.

[1] a) J. F. Larrow, E. N. Jacobsen, *Top. Organomet. Chem.* **2004**, *6*, 123–152; b) P. G. Cozzi, *Chem. Soc. Rev.* **2004**, *33*, 410–421; c) E. M. McGarrigle, D. G. Gilheany, *Chem. Rev.* **2005**, *105*, 1563–1602; d) D. A. Atwood, M. J. Harvey, *Chem. Rev.* **2001**, *101*, 37–52; e) D. J. Darensbourg, *Chem. Rev.* **2007**, *107*, 2388–2410; f) T. Katsuki, *Chem. Soc. Rev.* **2004**, *33*, 437–444; g) N. Madhavan, C. W. Jones, M. Weck, *Acc. Chem. Res.* **2008**, *41*, 1153–1165.

[2] a) S. J. Wezenberg, A. W. Kleij, *Angew. Chem. Int. Ed.* **2008**, *47*, 2354–2364; b) A. W. Kleij, *Chem. Eur. J.* **2008**, *14*, 10520–10529.

[3] a) P. D. Frischmann, J. Jiang, J. K.-H. Hui, J. J. Grzybowski, M. J. MacLachlan, *Org. Lett.* **2008**, *10*, 1255–1258; b) C. Ma, A. Lo, A. Abdolmaleki, M. J. MacLachlan, *Org. Lett.* **2004**, *6*, 3841–3844.

[4] S. J. Wezenberg, E. C. Escudero-Adán, J. Benet-Buchholz, A. W. Kleij, *Org. Lett.* **2008**, *10*, 3311–3314.

[5] See for instance: G. H. Clever, Y. Söltl, H. Burks, W. Spahl, T. Carell, *Chem. Eur. J.* **2006**, *12*, 8708–8718.

[6] a) P. Goyal, X. Zheng, M. Weck, *Adv. Synth. Catal.* **2008**, *350*, 1816–1822; b) C. Mazet, E. N. Jacobsen, *Angew. Chem. Int. Ed.* **2008**, *47*, 1762–1765.

[7] a) A. W. Kleij, M. Kuil, D. M. Tooke, A. L. Spek, J. N. H. Reek, *Inorg. Chem.* **2007**, *46*, 5829–5831; b) A. W. Kleij, M. Kuil, M. Lutz, D. M. Tooke, A. L. Spek, P. C. J. Kamer, P. W. N. M. van Leeuwen, J. N. H. Reek, *Inorg. Chim. Acta* **2006**, *359*, 1807–1814; c) E. C. Escudero-Adán, J. Benet-Buchholz, A. W. Kleij, *Inorg. Chem.* **2008**, *47*, 410–412; d) S. J. Wezenberg, E. C. Escudero-Adán, J. Benet-Buchholz, A. W. Kleij, *Inorg. Chem.* **2008**, *47*, 2925–2927.

[8] a) A. W. Kleij, D. M. Tooke, M. Lutz, A. L. Spek, J. N. H. Reek, *Eur. J. Inorg. Chem.* **2005**, 4626–4634; b) S. Curreli, E. C. Escudero-Adán, J. Benet-Buchholz, A. W. Kleij, *J. Org. Chem.* **2007**, *72*, 7018–7021; S. Curreli, E. C. Escudero-Adán, J. Benet-Buchholz, A. W. Kleij, *Eur. J. Inorg. Chem.* **2008**, 2863–2873.

[9] A. W. Kleij, D. M. Tooke, M. Kuil, M. Lutz, A. L. Spek, J. N. H. Reek, *Chem. Eur. J.* **2005**, *11*, 4743–4750.

[10] Recently we reported the isolation of four-coordinate Zn(salphen) species using a supramolecular strategy: E. C. Escudero-Adán, J. Benet-Buchholz, A. W. Kleij, *Chem. Eur. J.* **2009**, *15*, 4233–4237.

[11] A. Dalla Cort, L. Mandolini, C. Pasquini, K. Rissanen, L. Russo, L. Schiaffino, *New J. Chem.* **2007**, *31*, 1633–1638.

[12] See for an example: E. C. Escudero-Adán, J. Benet-Buchholz, A. W. Kleij, *Dalton Trans.* **2008**, 734–737.

[13] Please note the resemblance of the upfield shifts noted for the *ortho* protons of pyridine derivatives ligating to $Zn^{II}$-porphyrin systems. However, in the case of $Zn^{II}$-salphen complexes the magnitude of these displacements is generally much less abundant due to the absence of a strong ring current in this type of ligand. The pyridine ligation at $Zn^{II}$-salphen complexes **1**–**5** is dynamic and thus sharp resonances are observed in all cases under the NMR conditions employed. Typically 10–20 mM solutions were examined.

[14] For similar NMR features of Zn(salphen) complexes ligated by nicotine alkaloid donor ligands see: E. C. Escudero-Adán, J. Benet-Buchholz, A. W. Kleij, *Inorg. Chem.* **2008**, *47*, 4256–4263.

[15] See for software details: A. P. Bisson, C. A. Hunter, J. C. Morales, *Chem. Eur. J.* **1998**, *4*, 845–851.

[16] E. C. Escudero-Adán, J. Benet-Buchholz, A. W. Kleij, *Inorg. Chem.* **2007**, *46*, 7265–7267.

[17] L. San Felices, E. Escudero-Adán, J. Benet-Buchholz, A. W. Kleij, *Inorg. Chem.* **2009**, *48*, 846–853.

[18] K.-H. Chang, C.-C. Huang, Y.-H. Liu, Y.-H. Hu, P.-T. Chou, Y.-C. Lin, *Dalton Trans.* **2004**, 1731–1738.

[19] M.-A. Muñoz-Hernández, T. S. Keizer, S. Parkin, B. Patrick, D. A. Atwood, *Organometallics* **2000**, *19*, 4416–4421.

Received: May 4, 2009
Published Online: July 16, 2009

  